Thermoelectric materials: phase relationships and properties

Raul Cardoso-Gil[#], Matej Bobnar, Magnus Boström, Benoit Boucher, Wilder Carrillo-Cabrera, Felix Kaiser, Paul Simon, Igor Veremchuk, Frank R. Wagner, Xinke Wang, Iryna Zelenina, Yuri Grin

The better understanding of the relation between crystal chemistry, chemical bonding and electronic structure enables the interpretation and tuning of thermoelectric properties. Consequently, the interest was focused on the chemical insight of known and new thermoelectric materials based on intermetallic compounds, clathrates, oxides, as well as natural and synthetic chalcogenides.

***ht*-IrGa$_3$** [1], $CoGa_3$ and $RhGa_3$ are isoelectronic intermetallic compound with the $FeGa_3$ type of crystal structure. With 18 ve/fu, they are expected to show metallic character. However, in a recent theoretical study on this type of compounds, a band gap of ~0.14 eV was predicted for $IrGa_3$ [2], signing this compound as a potential thermoelectric (TE) material. For experimental evidence, single-phase *ht*-$IrGa_3$ was synthetized from the elements. It is a high temperature phase, forming peritectically from $IrGa_2$ and the melt at 970 °C and decomposing peritectoidally at 790 °C. The single crystal structure analysis shows huge anisotropy of the atomic displacement parameters after refinement in the $FeGa_3$ type (space group $P4_2/mnm$), indicating strong local disorder. The static nature of this disorder is evidenced by low temperature single crystal X-ray diffraction experiments. A model for the real crystal structure of tetragonal *ht*-$IrGa_3$ with splitting of the Ga positions is proposed. Atomic-resolution imaging study using TEM and STEM provides complementary information which supports the atomic arrangement proposed for the real structure of *ht*-$IrGa_3$.

The TE properties of *ht*-$IrGa_3$ show a semiconductor-like behavior of the temperature-dependent electrical resistivity, with a band gap of E_g = 0.03 eV. The Seebeck coefficient $S = -30\ \mu VK^{-1}$ up to 350 K, signs *ht*-$IrGa_3$ as an n-type semiconductor. A much lower |S| than that of $FeGa_3$ and $RuGa_3$ ($S_{290\,K} = -360\ \mu VK^{-1}$, $S_{300\,K} = -477\ \mu VK^{-1}$, respectively), is associated with a high charge carrier concentration $n \approx 10^{21}$ cm^{-3}. The lattice thermal conductivity at room temperature is lower than that of $FeGa_3$, $RuGa_3$ and $RuIn_3$, attained by the intrinsic structural disorder in *ht*-$IrGa_3$. The charge carrier concentration is optimized by the incorporation of holes, achieved by substituting Ga by Zn in the solid solution $IrGa_{3-x}Zn_x$ (x = 0.08, 0.16, 0.24, 0.32). An increase of the electrical resistivity and in the Seebeck coefficient is observed with growing zinc content. The thermal conductivity is noticeably reduced by the presence of additional phonon scattering centers. The hole-doping enhances *ZT* by only less than a factor of two with respect to the non-substituted material, being not enough to consider these materials as thermoelectric.

MoO_x [3] samples are exposed to reducing conditions during the high-temperature preparation ($T \leq 973$ K) in graphite-lined SPS dies. The phase formation in the bulk is not affected, allowing synthesis of single-phase materials with composition differences as low as Δx = 0.01 (≅ 0.07 at. % of oxygen). Thus, spark-plasma synthesis (SPS) is shown to be a suitable preparation method for single-phase oxide materials with well-defined composition in the system Mo – O.

The formation of $Mo_{18}O_{52}$ (x = 2.889), $Mo_{17}O_{47}$ (x = 2.760), and γ-Mo_4O_{11} (x = 2.750) is observed straightforwardly after successive synthesis steps. Due to decomposition of α-MoO_3 at elevated temperatures, SPS is constrained to $T_{max} \approx 973$ K in order to control the composition. This prevents the formation of high-temperature phases like Mo_9O_{28} (x = 2.889). The absence of η-Mo_4O_{11} (x = 2.750) may be influenced by an SPS-specific condition like the electric field.

Electrical and thermal transport properties have been determined for bulk polycrystalline samples of MoO_2, γ-Mo_4O_{11}, $Mo_{17}O_{47}$, and $Mo_{18}O_{52}$ between room temperature and 763 K. From the activation energy for electrical conduction of E_a = 0.30(3) eV, $Mo_{18}O_{52}$ is assumed to be a narrow-gap *p*-type semiconductor below 440 K. It shows exceptionally low thermal conductivity of $\kappa_{tot} \approx \kappa_{lat}$ = 0.5–0.9 Wm^{-1}K^{-1} in the whole temperature range. A large positive Seebeck coefficient of +140 μVK^{-1} is observed at room temperature. Above 440 K, a *p*–*n* transition occurs and the Seebeck coefficient is distinctly decreased (−38 μVK^{-1} at 763 K).

An encouraging $S = -70\ \mu VK^{-1}$ at 763 K and power factor ≈30 Wm^{-1}K^{-2} at 440 K ≤ T ≤ 610 K, are found for *n*-type $Mo_{17}O_{47}$. The resulting figure-of-merit *ZT* is still low for all MoO_x phases ($2 \leq x < 3$) with the following maxima: $ZT(763\ K) = 5 \times 10^{-3}$, 39×10^{-3}, 14×10^{-3} and $ZT(690\ K) = 0.9\ 10^{-3}$ for $Mo_{18}O_{52}$ (x = 2.889), $Mo_{17}O_{47}$ (x = 2.760), and γ-Mo_4O_{11} (x = 2.750) for MoO_2, respectively.

FeS_2 (Pyrite) [4, 5] is an earth-abundant mineral, which has been addressed as an auspicious thermoelectric material, due to its enhanced electrical properties, suitable energy-gap, non-toxicity and low-cost constituents. Also, geoscientific collections provided access to natural specimens with known geological precedence and of suitable characteristics for their study. The thermoelectric properties of natural and synthetic materials were well characterized, along with a mineralogical study of the natural specimens. To learn about the intrinsic transport properties of pyrites, both natural and synthetic single-phase bulk and single crystals of FeS_2 were studied. The high purity of the bulk synthetic sample was achieved by additional long annealing under sulfur vapors. A natural sample with geological origin in Saxony revealed to be of high purity. The study revealed both pyrites to be chemically stable under application-conditions up to ~600 K, with optimal Seebeck coefficient ($\sim -450\ \mu VK^{-1}$ at 600 K) and a high electrical resistivity ($220 - 5 \cdot 10^{-3}\ \Omega m$). Further studies revealed a high phonon-mediated thermal conductivity ($\sim 40 - 20\ Wm^{-1}K^{-1}$), to be improved for thermo-electric applications. Furthermore, according to theoretical calculations, substitution of S by As in FeS_2 results in a strong As−Fe interaction with orbital hybridization generating an additional valence band close to the Fermi level. To prove this result, **$FeAs_xS_{2-x}$** ($x \leq 0.1$) bulk samples were prepared and compared with arsenian pyrites of natural origin. The study revealed that $x = 0.1$ is the maximum As-solubility in bulk samples, with a reduction in the energy gap, a change from electron to hole-like conduction mechanism, as well as the enhancement of its TE properties. The S substitution by As reduced the phonon thermal conductivity by a factor of 2.

In_3S_4 [6-8] was studied, including a designing of the systematic routine to distinguish between the α- and β-polymorphic modifications, reinvestigation of their crystal structures and an analysis of the mechanism of the α-β phase transition. The temperature and compositional homogeneity ranges of both polymorphs, distribution of cations in the cubic spinel structure as well as electronic and thermal transport properties were studied within the binary $In_{1-x}\square_xIn_2S_4$, the ternary MIn_2S_4 (M = Mn, Fe, Co, Ni), $Fe_xIn_yS_4$, $In_{2.67}\square_{0.33}S_{4-x}Se_x$ and $In_{2.67}\square_{0.33}S_{4-y}Te_y$, as well as the quaternary $Fe_{1-x}Mn_xIn_2S_4$ systems.

Incorporation of an additional chemical element or substitution of indium or sulfur in the structure of $In_{0.67}\square_{0.33}In_2S_4$ favor the formation of disordered spinel phase at RT, sometimes preceded by a narrow homogeneity range of the β-polymorph and/or a two-phase region for low concentration of the introduced element. The strictly stoichiometric β-$In_{0.67}\square_{0.33}In_2S_4$ thiospinel can be obtained in sulfur-rich atmosphere, whereas synthesis in vacuum may lead to a small deviation from the nominal composition. Such an off-stoichiometry significantly influences electronic transport properties, especially the charge carrier mobility, which consequently leads to a two-fold improvement of $ZT_{max} \approx 0.2$ in the latter compound. These observations, together with a narrow stability range of the β-modification, exemplify the unique character of this tetragonal phase and its crystal structure.

The homogeneity range of the ternary $Fe_xIn_yS_4$ thiospinel was confirmed to be larger than the one previously reported and Fe atoms can be incorporated into pristine $In_{0.67}\square_{0.33}In_2S_4$ via at least three different schemes. Considering that MIn_2S_4 (M = Co, Ni) compounds adopt analogous *nearly-inverse* spinel structures, similarly broad stability ranges can be expected for them.

PbTe-based compounds [9], as one of the most investigated family of TE materials, have been developed into state-of-the-art *p*-type and *n*-type TE materials. However, there are quite a few studies focusing on the reproducibility of TE properties and microstructure evolution during different heat treatments. $Pb_{0.98-x}Na_{0.02}Eu_xTe$ (x = 0–0.030) samples were systematically examined after three different kinds of heat treatments: spark plasma sintering (SPS), laser flash measurement (LFA), and long-term annealing. The maximal solubility of Eu (*ca.* 1.0 at. %) in $Pb_{0.98-x}Na_{0.02}Eu_xTe$ was established at 873 K. A part of Eu becomes Eu^{3+} within the homogeneity range due to the charge compensation caused by Pb^{2+}-by-Na^{1+} substitution or by a change in the sample composition towards the Te-rich side. The most inhomogeneous samples (after SPS) show highest values of figure-of-merit, ZT_{max}, of up to 2.1 at 760 K, due to a large number of micrometer-scale sodium- and europium-rich aggregations within them. After additional heat treatment (LFA measurement or long-term annealing), the ZT_{max} value reduces to 1.6 (Fig. 1). The distribution of Eu and Na in the samples becomes much more homogeneous, accompanied by increased lattice parameters and decreased carrier concentrations. The long-term annealed samples have the best stable TE properties and good mechanical stability in the cyclic measurements. Surface protection needs to be considered for the temperatures above 773 K in order to avoid material decomposition. This study clearly demonstrates that out-of-equilibrium materials may

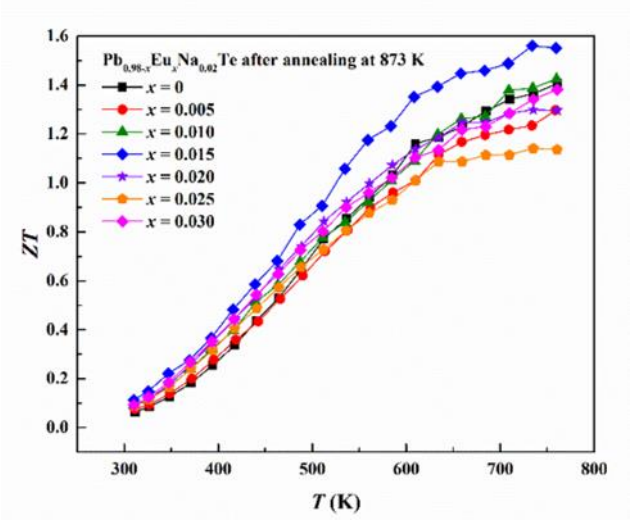

Fig. 1: Temperature dependence of the thermoelectric figure of merit ZT *for after 900 hours annealing at 873 K.*

have promising high *ZT* values under certain circumstances, but these *ZT* values will generally approach lower values after heat treatment similar to the "working conditions".

$PbGa_6Te_{10}$ [10] is a potential thermoelectric material due to its ultralow thermal conductivity and moderated values of the Seebeck coefficient. The study was focused on the characterization of thermal, structural, and microstructural properties of the Pb-Ga-Te ternary system around the $PbGa_6Te_{10}$ composition. Two series of polycrystalline samples with compositions $(PbTe)_{1-x}(Ga_2Te_3)_x$ ($0.67 \leq x \leq 0.87$) and $Pb_yGa_6Te_{10}$ ($0.85 \leq y \leq 1.5$) were synthesized and characterized. Differential scanning calorimetry measurements revealed that $PbGa_6Te_{10}$ melts incongruently at 1007 ± 2 K and has a polymorphic phase transition at 658 – 693 K depending on composition. Powder X-ray diffraction of annealed samples confirmed that below 658 K the trigonal modification of $PbGa_6Te_{10}$ exists (space group $P3_121$ or $P3_221$) and above 693 K the rhombohedral one (space group $R32$). A homogeneity range for $Pb_yGa_6Te_{10}$ was found for y = 0.9 - 1.1 based on refined lattice parameters of $Pb_yGa_6Te_{10}$ in samples annealed at 873 K. The revised version of the PbTe-Ga_2Te_3 phase diagram in the vicinity of the $PbGa_6Te_{10}$ phase was proposed. Furthermore, the TE properties of the $Pb_yGa_6Te_{10}$ samples were studied in detail considering the new results of the phase equilibria. The deviation from the stoichiometric composition leads to a tuning of the charge transport in $Pb_yGa_6Te_{10}$, proposing the effective engineering of the Seebeck coefficient and electrical conductivity over the homogeneity range. Pb-deficient $Pb_{0.9}Ga_6Te_{10}$ sample shows improved power factor up to 9.5 $\mu Wm^{-1}K^{-2}$ and reduced thermal conductivity as low as 0.17 $Wm^{-1}K^{-1}$ due to attuned chemical potential and additional scattering of phonons on point defects, respectively. Thus, the dimensionless thermoelectric figure of merit for this composition was improved up to almost 4 times compared to the stoichiometric specimen.

$Ba_{8-\delta}Au_xGe_{46-y}$ [11] is a type-I clathrate phase, whose thermoelectric properties were investigated for several sample compositions in the region $Ba_{7.8}Au_{5.33}Ge_{40.7}$. A maximum dimensionless thermoelectric figure of merit *ZT* of ≈ 0.9 at 670 K was reproducibly achieved (Fig. 2). An upscaled preparation procedure consisting of steel quenching and spark plasma sintering allowed for the fabrication of 40 module legs of 5 × 5 × 7 mm^3. Eight couples with the clathrate-I compounds $Ba_{7.8}Au_{5.33}Ge_{40.67}$ as *p*-type and $Ba_8Ga_{16}Ge_{30}$ as *n*-type material were integrated into a demonstrator module with an output power of 0.2 W (ΔT = 380 K; T_1 = 673 K, T_2 = 293 K).

Uranium-based materials were studied establishing them as possible candidates for extraterrestrial thermoelectric applications [12].

Analysis of the chemical bonding in thermoelectric and related materials was performed by quantum chemical techniques in position space [13]. The atomic interactions play a crucial role in the chemical and structural organization of thermoelectric materials, where bonding features are the significant reason for both the crystallographic complexity and the thermoelectric behavior. Chemical bonding forms the basis for the total electron balance in the material regulating electron concentration and transport

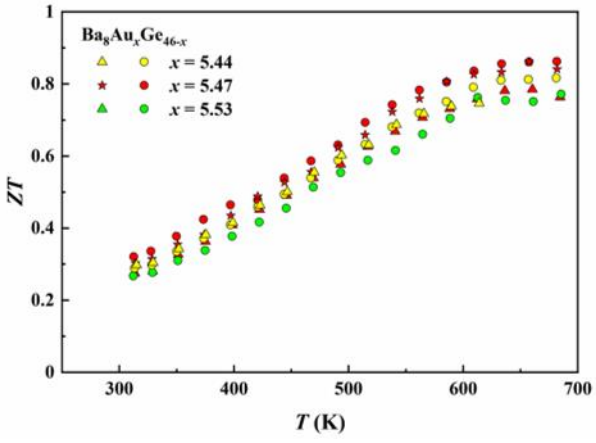

Fig. 2: Reproducibility of the thermoelectric properties of $Ba_8Au_xGe_{46-x}$ (x = 5.44, 5.47 and 5.53) for different batches with the same composition.

(electron engineering) as well as the heat transport in the material (phonon engineering). The three-dimensional distribution of structural regions with different types of chemical bonding – *inhomogeneity* and *anisotropy* of bonding – influences the thermal and electronic transport more than the crystallographic fingerprints only.

External Cooperation Partners

Roman Gumeniuk, Pawel Wyzga, Esteban Zuñiga-Puelles (TU Bergakademie, Freiberg, Germany); Lukyan Anatychuk (Institut of Thermoelectricity, Czerniutsi, Ukraine); Krzystof Wojciechowski, Oleksandr Cherniushok (AGH University, Krakow, Poland).

References

[1] *The intermetallic semiconductor $IrGa_3$: a material in the in-transformation state, R. Cardoso-Gil, I. Zelenina, Q.E. Stahl, M. Bobnar, I. Veremchuk, P. Simon, W. Carrillo-Cabrera, M. Boström, Yu. Grin, ACS Mater. Au (2021) submitted.*

[2] *Theoretical study of thermoelectric properties, B. Boucher, PhD Thesis, 2017, Universite Bretagne Loire, Rennes, France/Max-Planck-Institut für Chemische Physik fester Stoffe, Dresden, Germany.*

[3]* *Molybdenum Oxides MoO_x: Spark-Plasma Synthesis and Thermoelectric Properties at Elevated Temperature, F. Kaiser, M. Schmidt, Yu. Grin, I. Veremchuk, Chem. Mater.* ***32*** *(2020) 2025, doi.org/10.1021/acs.chemmater.9b05075*

[4]* *Structural stability and thermoelectric performance of high quality synthetic and natural pyrites (FeS_2), E. Zuñiga-Puelles, R. Cardoso-Gil, M. Bobnar, I. Veremchuk, C. Himcinschi, C. Kortus, G. Heide, R. Gumeniuk, Dalton Trans.* ***48*** *(2019) 10703, doi.org/10.1039/c9dt01902b*

[5]* *Electrical and thermal transport properties of natural and synthetic $FeAs_xS_{2-x}$ ($x =\leq 0.01$), E. Zuñiga-Puelles, R. Cardoso-Gil, M. Bobnar, I. Veremchuk, G. Heide, R. Gumeniuk, J. Phys. Chem. Solids* ***150*** *(2021) 109809, doi.org/10.1016/j.jpcs.2020.109809*

[6]* *Indium thiospinel $In_{1-x}\square_x In_2S_4$–structural characterization and thermoelectric properties, P. Wyzga, I. Veremchuk, C. Himcinschi, U. Burkhardt, W. Carrillo-Cabrera, M. Bobnar, C. Henning, A. Leithe-Jasper, J. Kortus, R. Gumeniuk, Dalton Trans.* ***48*** *(2019) 8350, doi.org/10.1039/c9dt00890j*

[7]* *Structural peculiarities and thermoelectric study of iron indium thiospinel, P. Wyzga, I. Veremchuk, M. Bobnar, P. Kozelj, S. Klenner, R. Pöttgen. A. Leithe-Jasper, R. Gumeniuk, Chem. Eur. J.* ***26*** *(2020) 5245, doi.org/10.1002/chem.201905665*

[8]* *Ternary MIn_2S_4 (M = Mn, Fe, Co, Ni) Thiospinels - Crystal Structure and Thermoelectric Properties, P. Wyzga, I. Veremchuk, M. Bobnar, C. Henning, A. Leithe-Jasper, R. Gumniuk, Z. Anorg. Allg. Chem.* ***646*** *(2020) 1091, doi.org/10.1002/zaac.202000014*

[9]* *Thermoelectric stability of Eu- and Na-substituted PbTe, X. Wang, I. Veremchuk, U. Burkhardt, M. Bobnar, H. Boethner, C.-Y. Kuo, C.T. Chen, C.-F. Chang, J.-T. Zhao, Yu. Grin, J. Mater. Chem. C* ***6*** *(2018) 9482, doi.org/10.1039/c8tc03142h*

[10]* *Phase equilibria and thermoelectric properties in the Pb-Ga-Te system in the vicinity of the $PbGa_6Te_{10}$ phase, O. Cherniushuk, R. Cardoso-Gil, T. Parashchuk, Yu. Grin, K. Wojciechowski, Inorg. Chem.* ***60*** *(2021) 2771, doi.org/10.1021/acs.inorgchem.0c03549*

[11] *Thermoelectric characterization of the clathrate-I solid solution $Ba_{8-\delta}Au_xGe_{46-x}$, M. Baitinger, H.-D. Nguyen, C. Candolfi, I. Antonyshyn, K. Meier-Kirchner, I. Veremchuk, V. Razinkov, M. Havryluk, R. Cardoso-Gil, U. Burkhardt, B. Böhme, L. Anatychuk, Yu. Grin, Applied Physics Letters (2021) accepted.*

[12] *Status Report 2021, 1.7 Minerva Group (E. Svanidze), p. 47.*

[13]* *Inhomogeneity and anisotropy of chemical bonding and thermoelectric properties of materials, Yu. Grin, J. Solid State Chem.* ***274*** *(2019) 329-336.*

[#] cardoso@cpfs.mpg.de